

## THE CORES OF DARK MATTER-DOMINATED GALAXIES: THEORY VERSUS OBSERVATIONS

ANDREY V. KRAVTSOV AND ANATOLY A. KLYPIN

Astronomy Department, New Mexico State University, Las Cruces, NM 88003-0001, USA

AND

JAMES S. BULLOCK AND JOEL R. PRIMACK

Physics Department, University of California, Santa Cruz, CA 95064

to be published in July 20, 1998 issue of the Astrophysical Journal

### ABSTRACT

We use the rotation curves of a sample of dark matter dominated dwarf and low-surface brightness (LSB) late-type galaxies to study their radial mass distributions. We find that the shape of the rotation curves is remarkably similar for all (both dwarf and LSB) galaxies in the sample, suggesting a self-similar density distribution of their dark matter (DM) halos. This shape can be reproduced well by a density profile with a shallow central cusp [ $\rho(r) \propto 1/r^\gamma$ ,  $\gamma \approx 0.2 - 0.4$ ] corresponding to a steeply rising velocity curve [ $v(r) \propto r^g$ ,  $g \approx 0.9 - 0.8$ ]. We further show that the observed shapes of the rotation curves are well matched by the average density profiles of dark matter halos formed in very high resolution simulations of the standard cold dark matter model (CDM), the low-density CDM model with cosmological constant ( $\Lambda$ CDM), and the cold+hot dark matter model with two types of neutrino (CHDM). This is surprising in light of several previous studies, which suggested that the structure of simulated dark matter halos is inconsistent with the dynamics of dwarf galaxies. We discuss possible explanations for this discrepancy and show that it is most likely due to the systematic differences at small radii between the analytic model proposed by Navarro, Frenk, & White, with  $\gamma_{\text{NFW}} = 1$ , and the actual central density profiles of the dark matter halos. We also show that the mass distributions in the hierarchically formed halos are *on average* consistent with the shape of rotation curves of dark matter dominated galaxies. However, the scatter of the individual profiles around the average is substantial. Finally, we show that the dark matter halos in our hierarchical simulations and the real galaxies in our sample exhibit a similar decrease in their characteristic densities with increasing characteristic radial scales and show increase in their maximum rotation velocities with increase in the radii at which their maximum velocities occur.

*Subject headings:* cosmology: theory – dark matter: halos — galaxies: kinematics and dynamics — galaxies: structure

### 1. INTRODUCTION

The amount of luminous matter (stars and gas) in many spiral and irregular galaxies is not sufficient to explain the amplitude and shape of their rotation curves (RCs). This discrepancy is usually interpreted as evidence for the presence of an extended dark matter (DM) halo surrounding the visible regions of galaxies (e.g., Casertano & van Gorkom 1991; Persic, Salucci, & Stel 1996, and references therein). The extent of the dark matter halos, estimated using satellite dynamics, is<sup>1</sup>  $\sim 0.2 - 0.5h^{-1}$  Mpc (Zaritsky & White 1994; Carignan et al. 1997; Zaritsky et al. 1997). However, the dynamical contribution of the dark matter can be substantial even in the very inner regions of galaxies: the observed rotation velocities of some dwarf and low-surface brightness (LSB) galaxies imply that DM constitutes a dominant fraction (up to  $\sim 95\%$ ) of dynamical mass within the last measured point of their RCs (e.g., Carignan & Freeman 1988; Martimbeau, Carignan, & Roy 1994; de Blok & McGaugh 1997). These *dark matter dominated galaxies* offer a unique opportunity for probing *directly* the density structure of DM halos which can be then compared with predictions of theoretical models.

The detailed structure of DM halos formed via dissipa-

tionless hierarchical collapse in CDM-like models was recently studied using high-resolution  $N$ -body simulations (Dubinski & Carlberg 1991; Navarro, Frenk, & White 1996, 1997, hereafter NFW96 and NFW97). The halo density profiles were found to be cuspy (coreless) and well fitted by the following two-parameter profile (NFW96):

$$\rho_{\text{NFW}}(r) = \frac{\rho_s}{(r/r_s)(1+r/r_s)^2}. \quad (1)$$

The characteristic density,  $\rho_s$ , and radius,  $r_s$ , are sensitive to the epoch of halo formation and are tightly correlated with the halo virial mass (NFW 96,97). Therefore, the results of these simulations suggest a coreless and self-similar density structure of DM halos, with the virial mass being the single scaling parameter.

The structure of the inner regions of galactic halos was studied by Flores & Primack (1994) and Moore (1994), who used high-resolution rotation curve measurements of several dark matter dominated dwarf galaxies. The central density distributions in these galaxies were found to be inconsistent with the singular [ $\rho(r) \propto 1/r$ ] behavior predicted by equation (1). The scaling properties of the observed halos were analyzed by Burkert (1995, hereafter

<sup>1</sup>We assume that the present-day value of the Hubble constant is  $H_0 = 100h$  km/s/Mpc.

B95), who pointed out that shapes of the density profiles of four dwarf galaxies analyzed by Moore (1994) are remarkably similar and are well fitted by the following phenomenological density profile:

$$\rho_B(r) = \frac{\rho_b}{(1 + r/r_b)[1 + (r/r_b)^2]}. \quad (2)$$

Parameters  $\rho_b$  and  $r_b$  were found to be strongly correlated, in qualitative agreement with the predictions of hierarchical models (B95).

In this paper we study the observed density structure in a sample of dark matter dominated galaxies inferred from their rotation curves. Particularly, we test two predictions of previous simulations of hierarchical halo formation: (1) cuspy central density distribution and (2) self-similarity of the halo density structure. We then use results of high-resolution  $N$ -body simulations to compare the observed rotation curves with circular velocity profiles of dark matter halos formed in different structure formation models.

## 2. DWARF AND LSB GALAXIES

### 2.1. The sample

We have compiled a sample of 10 dwarf and 7 LSB galaxies with measured rotation curves and published mass models for stellar, gas, and halo components (see Table 1). The dwarf galaxies were selected from different sources, whereas all 7 LSB galaxies were selected from the sample of de Blok, McGaugh, & van der Hulst (1996) (see Table 1).

In our sample we included only those galaxies in which the dark matter component was shown to constitute  $\gtrsim 85\%$  of the total mass inside the last measured point of the rotation curve (in most cases with the maximum disk assumption). It is important to note that distances to all of the dwarf, and some of the nearby LSB, galaxies are quite uncertain (in some cases by a factor of two). While rotational velocity is a directly observable quantity, the physical scale of rotation curves must be computed from the angular scale using distance. Thus, any uncertainty in the distance propagates into uncertainty in the physical scale. This fact should be kept in mind when one makes a one-to-one comparison of observed and modeled rotation curves. The distances to the galaxies adopted in our analysis are listed in Table 1. We have adopted the best estimate of distance from the original paper, when it was available, or the distance quoted in Tully (1988). We have also included in Table 1 the best fit values of mass model parameters described in §2.2.

### 2.2. Rotation curve analysis

Analysis of the dark matter distribution is difficult in most galaxies due to ambiguities in the estimates of the stellar mass-to-light ( $M/L$ ) ratios and the resulting dynamical contribution of the stellar component to the observed rotation velocities (e.g., de Blok & McGaugh 1997; Bottema 1997; Courteau & Rix 1997; and references therein). However, the rotation curves of the galaxies in our sample are mostly determined by dark matter on scales  $\gtrsim 1$  kpc: the contribution from the gas and stars is negligible and residuals between the observed rotation curves

and contribution of DM are at the level of the observational scatter of rotational velocities. Therefore, the dark matter distribution models can be directly fitted to the rotation curves of these galaxies without uncertain assumptions about  $M/L$  ratios.

B95 showed that the density distribution,  $\rho_B(r)$ , described by equation (2) fits the data very well over the entire observed range of scales. At large radii this profile falls off as  $\rho(r) \propto r^{-3}$ , in accord with simulations of the CDM model (e.g., NFW96). However, the change of logarithmic slope at  $r \sim r_0$  predicted by  $\rho_B(r)$ , equation (2), is faster than the change predicted by  $\rho_{\text{NFW}}(r)$ , equation (1). Moreover,  $\rho_B(r)$  has a flat core at small radii ( $r \ll r_b$ ), in disagreement with the  $r^{-1}$  central cusp of  $\rho_{\text{NFW}}(r)$ . For dwarf galaxies, the scale at which the density distribution is expected to become flat is quite small ( $\lesssim 1$  kpc) and is in fact below the current observational resolution. From a theoretical point of view the existence of a core is difficult to understand because hierarchical formation of halos is much more likely to result in cuspy central density distributions (Syer & White 1997). Therefore, we will consider the broader family of density profiles (Zhao 1996):

$$\rho(r) = \frac{\rho_0}{(r/r_0)^\gamma [1 + (r/r_0)^\alpha]^{(\beta-\gamma)/\alpha}}. \quad (3)$$

Note that  $\rho(r \ll r_0) \propto r^{-\gamma}$ ,  $\rho(r \gg r_0) \propto r^{-\beta}$ , and  $\alpha$  characterizes the sharpness of the change in logarithmic slope. This family includes both cuspy profiles of the type proposed by NFW96 ( $\alpha, \beta, \gamma = (1, 3, 1)$ ) and the so-called modified isothermal profile ( $\alpha, \beta, \gamma = (2, 2, 0)$ ), which is the most widely used model for the halo density distribution in analyses of observed rotation curves. It is also convenient to make direct fits with an analytic model similar to (3) for the velocity profile:

$$V(r) = V_t \frac{(r/r_t)^g}{[1 + (r/r_t)^\alpha]^{(g+b)/a}}, \quad (4)$$

where  $r_t$  and  $V_t$  are the effective ‘‘turnover’’ radius and velocity and  $a$  parameterizes the sharpness of the turnover. The limiting behaviors are  $V(r \gg r_t) \propto 1/r^b$  and  $V(r \ll r_t) \propto r^g$ . The peak of the velocity profile (4) occurs at the radius  $r_{\text{max}} = r_t(g/b)^{1/a}$ , and  $V_{\text{max}} = V(r_{\text{max}}) = V_t(g/b)^{g/a} [1 + g/b]^{-(b+g)/a}$ .

The existing rotation curve measurements, due to their finite resolution and extent, cannot be used to constrain all five parameters of the profiles (3) and (4). The inner radii of the observational rotation curves are well probed, so we can make a meaningful comparison with fitting functions having different inner density profiles  $\gamma$ . However, most of the galaxies in our sample have rotation curves that have not begun to decline at the outermost measured point and thus have very little information about the asymptotic slopes  $\beta, b$ . Given the uncertainties, we fix the outer logarithmic slope to the value suggested by the models<sup>2</sup> (1) and (2):  $\beta = 3, b = 0.34$ . Note, however, that as was noted by Burkert (1995) this value is also favored (to  $\beta = 2$  of the pseudo-isothermal profile) by *observed* highest quality rotation curves of dwarf galaxies. For the same reason, the sharpness of the turnover,  $\alpha$  or  $a$ , are not

<sup>2</sup> $V_{\text{NFW}}(r) \propto \sqrt{\ln r/r}$  for large  $r$ , which has an approximate slope of  $b \sim 0.34$  for values of  $r$  near a typical virial radius.

TABLE 1  
THE SAMPLE OF DWARF AND LSB GALAXIES

Galaxy (1)	$M_B$ (2)	$r_0$ $h^{-1}\text{kpc}$ (3)	$V_0$ $\text{km s}^{-1}$ (4)	$\rho_0$ $10^8 h^3 M_\odot \text{kpc}^{-3}$ (5)	$r_t$ $h^{-1}\text{kpc}$ (6)	$V_t$ $\text{km s}^{-1}$ (7)	$r_{max}$ $h^{-1}\text{kpc}$ (8)	$V_{max}$ $\text{km s}^{-1}$ (9)	Distance $h^{-1}\text{Mpc}$ (10)	Reference (11)
Dwarf										
DDO 154	-13.8	2.0	38	0.33	2.9	76	5.6	47	3.0	1,2
DDO 170	-15.2	4.4	52	0.13	6.5	105	12.4	64	14	3
NGC 2915	-16.8	1.1	69	3.77	1.7	140	3.2	86	2.5	4
IC 2574	-15.7	5.1	65	0.15	8.2	138	15.6	85	2.0	5
NGC 5585	-17.5	2.3	73	0.93	3.4	148	6.5	91	4.7	6
DDO 236	-16.8	4.4	59	0.16	6.8	122	13.1	75	1.4	7
DDO 7	-17.7	3.8	87	0.49	5.5	176	10.5	108	18	8
DDO 10	-16.3	3.5	54	0.23	5.3	112	10.0	69	7.8	8
UGC 2684	-13.7	1.6	41	0.59	2.6	86	4.9	53	4.1	8
DDO 34	-15.7	1.5	54	1.29	2.1	109	4.0	67	5.9	8
LSB										
F568-1	-17.5	3.8	97	0.61	5.5	197	10.5	121	64	9
F568-3	-17.7	6.1	96	0.23	9.1	196	17.4	121	58	9
F568-V1	-17.3	4.9	96	0.36	7.2	194	13.7	119	60	9
F571-8	-17.0	6.8	121	0.30	10.1	248	19.4	153	36	9
F574-1	-17.8	8.8	95	0.11	13.6	197	25.9	121	72	9
F583-1	-15.9	4.6	71	0.22	6.7	143	12.8	88	24	9
F583-4	-16.3	6.0	64	0.11	9.3	133	17.8	82	37	9

NOTES.— Col.(2)  $M_B$ , blue absolute magnitude; col.(3) best fit  $r_0$ (see eq. [3]; the fitting procedure is described in §2.2); col.(4)  $V_0 = V(r_0)$ ; col.(5) best fit  $\rho_0$  (see eq.[3]); col.(6) best fit  $r_t$  (see eq.[4]); col.(7) best fit  $V_t$  (see eq.[4]); col.(8)  $r_{max}$ ; col.(9)  $V_{max} = V(r_{max})$ ; col.(10) distance to galaxy adopted in this study;

REFERENCES.— (1) Carignan & Freeman 1988; (2) Carignan & Beaulieu 1989; (3) Lake et al. 1990; (4) Meurer et al. 1996; (5) Martimbeau et al. 1994; (6) Côté et al. 1991; (7) Jobin M. & Carignan C. 1990; (8) van Zee et al. 1997; (9) de Blok et al. 1996.

constrained for all of the galaxies. However, a fair number of galaxies in the sample do show the turnover and thus can be used to constrain  $\alpha$ . The plausible value of the parameter  $\alpha = 2$  was determined using rotation curves of these galaxies. We generalize this value to all of the galaxies (which in no way contradicts the data, but is not, of course, a strict procedure) and thus currently we can only talk about a plausible range of  $\alpha$  values as a “universal fit” (if any such universal value exist at all). For example, our results will not change drastically if we use  $\alpha = 1.5$  instead of  $\alpha = 2$ . However,  $\alpha = 1$  gives a poorer fit to the data.

We fix the parameter  $\gamma$  to 0.2: the value which best fits most of the observed rotation curves.

The corresponding best-fit slopes of the profile (4) are  $(a, b, g) = (1.50, 0.34, 0.9)$ . Note that  $g = 1 - \gamma/2$ . With parameters  $\alpha, \beta$ , and  $\gamma$  ( $a, b, g$ ) fixed, we fitted the data for the remaining free parameters of the profile (3):  $\rho_0$  and  $r_0$  ( $V_t$  and  $r_t$  in eq.[4]). Our fits thus have the same number of free parameters as do profiles (1) and (2). Note that while the particular set of the parameters  $(\alpha, \beta, \gamma) = (2, 3, 0.2)$  used in the paper didn’t result from a strict fitting procedure, it was motivated by all possible constraints of available data. The only theoretically suggested value is that of  $\beta$  but it also seems to be favored by data (Burkert 1995). Hopefully, as new RC observations come along, they can be used to pinpoint the parameters  $\alpha$  and  $\beta$  with a better accuracy.

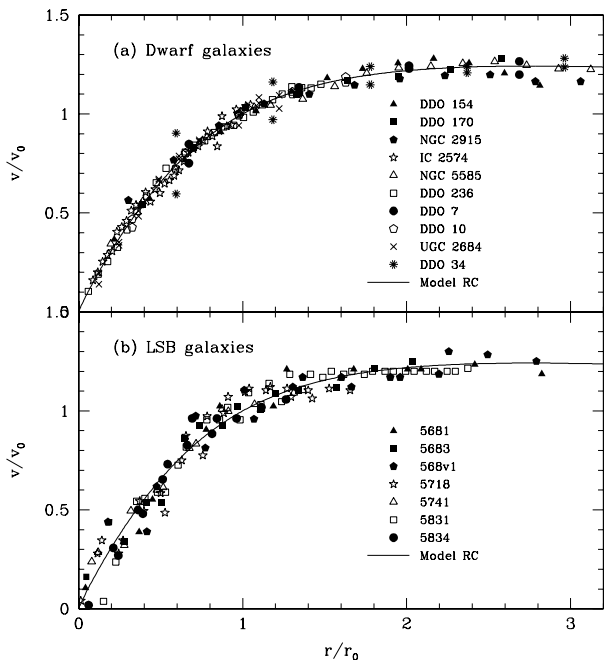


FIG. 1.—Rotation curves of (a) dwarf and (b) LSB galaxies (symbols) normalized to the best fit values of  $r_0$  and rotational velocities  $v_0$  at  $r_0$  predicted by density model (eq.[3]). The solid line on both panels shows the analytic rotation curve corresponding to the density profile (eq.[3]) with  $(\alpha, \beta, \gamma) = (2, 3, 0.2)$ . The rotation curves for different dwarf and LSB galaxies have virtually identical shapes, which is very well matched over the entire observed range of scales by the analytic model. Note, that the RC of NGC 2915 extends outside the scale of the plot: the outer part of this RC can be seen in Figure 2.

<sup>3</sup>By the *shape* of a rotation curve we mean its particular functional form. For example, the shape of the rotation curve described by equation (4) is  $x^g/(1+x^a)^{(g+b)/a}$  (where  $x \equiv r/r_t$ ). By saying that the RC shape is similar for all our galaxies, we mean that all their rotation curves can be described by this functional form with fixed values of parameters  $a, b$ , and  $g$ .

Figure 1 shows rotation curves of dwarf (a) and LSB (b) galaxies normalized to their best fit values of  $r_0$  and to the rotational velocities  $v_0$  at  $r_0$ , predicted by analytic profile (3). The best fit values of  $r_0, \rho_0, V_0 = V(r_0), r_t$ , and  $V_t$  are given in Table 1 for each galaxy in the sample. The formal errors of each of these values are less than about  $\sim 2 - 5\%$ . Figure 1a shows that all of the dwarf galaxies have rotation curves of virtually identical shape<sup>3</sup> with a remarkably small scatter. The rotation curves of the two dwarf galaxies, DDO154 and NGC2915, cannot be described by a smooth density distribution model in their outer parts. The RC of DDO154 shows a decrease in rotational velocity in the three outermost observed points. Conversely, the RC of NGC2915 has a sharp upturn at  $\gtrsim 5h^{-1}$  kpc (or  $r/r_0 \gtrsim 4.5$ ). This upturn can be seen in Figure 2. The explanation of this peculiar behavior is not clear (see, however, Burkert & Silk 1997), but it is obvious that it cannot be explained by any smooth model for the mass distribution. Note, however, that apart from the peculiar outer regions, the rotation curves of both DDO154 and NGC2915 have the same shape as the rest of the galaxies.

The shape of the galaxies’ rotation curves is well matched by the rotation curve corresponding to density profile (3) with  $(\alpha, \beta, \gamma) = (2, 3, 0.2)$  or correspondingly to RC (4) with  $(a, b, g) = (1.5, 0.34, 0.9)$ . This result is in perfect agreement with Burkert (1995) who showed similarity of rotation curves for four dwarf galaxies (two of which, DDO154 and DDO170, were included in our sample). As was mentioned above, the similar fit by  $\rho_B(r)$  (eq. [2]) proposed by Burkert (1995) is equally good. Note, however, that our profile does not have any flat core, whereas  $\rho_B(r)$  predicts such a core at  $r \ll r_b$ . The fact that both profiles fit the data equally well is easy to understand if we notice that  $\rho_B(r)$  predicts a flat density distribution at the scales well below the observational resolution ( $\lesssim 1$  kpc). Thus,  $\rho_B(r)$  and profile (3) can be virtually identical in the range of scales resolved in observations and thus provide an equally good fit to the data.

Figure 1b shows that the rotation curves of dark matter dominated LSB galaxies are also well described by the *same* analytic density profile. The larger amplitude of scatter in the case of LSB galaxies can be explained by the larger observational errors associated with a given point of a rotation curve and thus most likely reflects observational uncertainties rather than intrinsic scatter of the halo properties. Most of the LSB galaxies in our sample are located at considerably larger distances than dwarf galaxies. Therefore, the dwarf galaxies have been observed with considerably higher resolution and smaller observational errors than LSB galaxies. The estimated errors are typically 10 – 20% (de Blok et al. 1996), especially in the inner regions of galaxies ( $\lesssim 10$  kpc).

One important issue is whether subtraction of baryon component (stars and gas) in the galaxies from our sample will affect results of the rotation curve analysis presented above. As we mentioned in §2.1, the combined contribution of stars and gas is  $\lesssim 15\%$  for all of our galaxies ( $\lesssim 10\%$  in most cases). It is clear that ideally one has to subtract

contributions of both gas and stars from the observed RC in order to get the mass distribution of the dark matter to an accuracy of better than 10%. However, it is well known that this is not an easy thing to do. For stars, the exact mass-to-light ratio is not known and we cannot convert visible flux into the stellar mass without making additional assumptions (hence, “maximum disk controversy”). In the case of gas, we know exactly how to convert the 21-cm flux into the mass of gas (no mass-to-light uncertainty). This conversion, however, relies on other assumptions which can easily lead to uncertainties as high as 10% in the contribution of gas. For example, we need to know distance to the galaxy in order to make this conversion. We also need to have a reliable way to estimate the profile of molecular gas to recover the dark matter density profile. The distances to the dwarf galaxies in our sample are *very* uncertain (often by a factor of two or more) and so is the conversion. It is not clear whether it makes any sense to subtract the gas with uncertainties of its contribution this big. After all, the motivation for use of dark matter dominated galaxies for this kind of analysis is to avoid dubious or uncertain correction procedures which are very unlikely to result in a better determination of the shape of DM density distribution. The distance uncertainty is not so severe for LSB galaxies and so conversion could, in principle, have been done in this case. We have not done this for one simple reason: subtraction of the gas component could change any given point of rotation curve by at most 10% (in practice less than that). However, the errors associated with each point of RC are of the order of 10 – 20% (which combine both observational errors and asymmetries in the rotation curves between receding and approaching sides) and it seems unlikely that correction due to gas subtraction would improve or systematically change the answer (unless the observational errors are significantly overestimated). We have tested the effect of gas subtraction on the RC shapes by performing RC shape analysis for two galaxies (dwarf NGC 5585 and LSB F583 – 1) with and without subtraction of gas. The two galaxies have been selected to have a clearly visible turnover of the RC and to have a fairly high fraction of gas inside the last measured point of the rotation curve. This fraction is 8% for NGC 5585 (Côte et al. 1991) and 5% for F583 – 1 (de Blok et al. 1996). The results of fitting the  $(\alpha, \beta, \gamma) = (2.0, 3.0, 0.2)$  model to the RC with and without gas subtraction result in very similar results: the difference in the best fit parameters is  $\lesssim 10\%$  and corrected and uncorrected RCs have virtually identical shape. Note also that the dwarf galaxies that we used have on average a higher (or at least as high) fraction of gas (typically  $\sim 6 - 10\%$ ) than LSB galaxies (typically 3 – 7%). Therefore, if gas would introduce systematic differences in the shape of RC, we could expect that the scatter in Figure 1 to be larger for dwarf galaxies (some galaxies have much more gas than the others). Yet, the shape of rotation curves for dwarf galaxies is very uniform.

We have repeated the fitting procedure described above using the analytic profiles (1) and (2). As was mentioned above,  $\rho_B(r)$  results in a fit that is equally good to the fit by profile (3) shown in Figure 1. However, the analytic profile proposed by NFW failed to produce a reasonable fit to the data, as was indeed pointed out in NFW96 (see their fig.12). The major difficulty with this profile, as was

noted before by Flores & Primack 1994 and B95, is that the inner slope of the density distribution ( $\gamma = 1$ ) is considerably steeper than implied by the rotation curves. The finite spatial extent of the data and incorrect inner slope of the profile (1) lead to implausible solutions of the  $\chi^2$ -minimization procedure (the values of  $r_s$  increase without convergence).

The observed similarity of the shapes of the rotation curves for seventeen different galaxies, selected solely on the basis of their dark matter content, and the remarkably small amount of scatter, implies that their matter distributions are *self-similar* in terms of the density structure. Of course, this includes both stellar and gaseous matter as well as DM. Both stellar and gaseous masses are uncertain because of uncertainties in the distance, mass-to-light ratio, and atomic-to-molecular gas ratio of each galaxy. To the extent that we can neglect the stellar and gaseous components (a subject that we intend to address in a subsequent paper), the self-similar rotation curves of these DM-dominated galaxies imply that they all have the same density structure. The question we now ask is whether the disagreement between this density structure and  $\rho_{\text{NFW}}(r)$  indicates a failure of CDM-type models?

### 3. COMPARISON WITH THEORETICAL MODELS

#### 3.1. Numerical simulations

We have used the new Adaptive Refinement Tree (ART)  $N$ -body code (see Kravtsov, Klypin, & Khokhlov 1997 for details) to simulate the evolution of collisionless dark matter in the three cosmological structure formation models: (1) standard cold dark matter model (CDM:  $\Omega_0 = 1$ ,  $h = 0.5$ ,  $\sigma_8 = 0.7$ ); (2) a low-density CDM model with cosmological constant ( $\Lambda$ CDM:  $\Omega_\Lambda = 0.7$ ,  $h = 0.7$ ,  $\sigma_8 = 1.0$ ); and (3) a cold+hot dark matter model with two types of neutrino (CHDM;  $\Omega_0 = 1$  and  $\Omega_\nu = 0.2$ ;  $h = 0.5$ ;  $\sigma_8 = 0.7$ ; cf. Primack et al. 1995). Here  $\Omega_0$ ,  $\Omega_\Lambda$ , and  $\Omega_\nu$  are the present-epoch values of the density of matter, vacuum energy (as measured by the cosmological constant), and massive neutrinos, respectively. The rms fluctuation in spheres of radius  $8h^{-1}$  Mpc,  $\sigma_8$ , was chosen to conform with the local abundance of galaxy clusters, for  $\Lambda$ CDM and CHDM models it is also in agreement with measurements of the cosmic microwave background anisotropy by the *COBE* satellite. The simulations followed trajectories of  $128^3$  cold dark matter particles in a box of size of  $L_{\text{box}} = 7.5h^{-1}$  Mpc. In the CHDM simulation, two additional equal-mass “massive neutrino” species were evolved, which brings the number of particles in the simulation to  $3 \times 128^3$ . To test for the possible effects of the finite box size, we have run an additional simulation of the  $\Lambda$ CDM model with the box size twice as large:  $L_{\text{box}} = 15h^{-1}$  Mpc = 21.43 Mpc. We will denote the two  $\Lambda$ CDM simulations as  $\Lambda\text{CDM}_{7.5}$  and  $\Lambda\text{CDM}_{15}$  according to their box sizes.

We have used a  $256^3$  uniform grid covering the entire computational volume and finer refinement meshes constructed recursively and adaptively inside the high-density regions. The *comoving* cell size corresponding to a refinement level  $L$  is  $\Delta x_L = \Delta x_0 / 2^L$ , where  $\Delta x_0 = L_{\text{box}} / 256$  is the size of the uniform grid cell ( $L = 0$  corresponds to the uniform grid). The increase of spatial resolution corresponding to each successive refinement level was accompa-

nied by the decrease of the integration time step by a factor of 2. The simulations were started at redshift  $z_i = 40$  in the CDM and  $\Lambda$ CDM<sub>7.5</sub> simulations and at  $z_i = 30$  in the CHDM and  $\Lambda$ CDM<sub>15</sub> simulations. Particle trajectories were integrated with the time step of  $\Delta a_0 = 0.0015$  on the zeroth-level uniform grid in the case of the CDM and  $\Lambda$ CDM runs and with  $\Delta a_0 = 0.006$  in the CHDM run. The time step on a refinement level  $L$  is  $\Delta a_L = \Delta a_0 / 2^L$ . The time step for the highest refinement level corresponds to  $\gtrsim 40,000$  time steps over the Hubble time. Six refinement levels were introduced in the highest density regions corresponding to a cell size of  $\Delta x_6 = 0.46h^{-1}$  kpc. The *dynamic range* of the simulations is thus  $256 \times 2^6 = 16,384$ . Note, that the resolution is *constant in comoving coordinates* which means that actual physical resolution is higher at earlier epochs (the halos were resolved with six refinement levels as early as  $z \approx 1$ ). The refinement criterion was based on the local overdensity of dark matter particles. Regions with overdensity higher than  $\delta = n_{th}(L) 2^{3(L+1)}$  were refined to the refinement level  $L$ . Here,  $n_{th}(L)$  is the threshold number of particles per mesh cell of level  $L$  estimated using the cloud-in-cell method (Hockney & Eastwood 1981). We have used values  $n_{th} = 5$  at all levels in the CDM and  $\Lambda$ CDM runs; for the CHDM run we have used  $n_{th} = 10$  at the levels  $L = 0, 1$  and  $n_{th} = 5$  for all of the higher levels. These values of threshold were suggested by results of the tests presented in Kravtsov et al. (1997); they ensure that refinements are introduced only in the regions of high-particle density, where the two-body relaxation effects are not important.

For the dark matter halos used in our analysis the spatial resolution is equal to  $\approx 0.5 - 2h^{-1}$  kpc (corresponding to the 6th to 4th refinement levels). For each of the analyzed halos, we have taken into account only those regions of the density and circular velocity profiles that correspond to scales at least twice as large as the formal resolution. The mass resolutions (particle mass) of our simulations are listed in Table 2, and are in the range of  $\sim (1-10) \times 10^7 h^{-1} M_\odot$ . Therefore a typical halo of mass  $\sim 10^{11} h^{-1} M_\odot$  in our simulations contains several thousands of particles.

These simulations are comparable in spatial and mass resolution, as well as in the box size, to those of NFW96,97. There is, however, a significant difference: our simulations are direct simulations of *all* DM halos in a given computational volume, whereas NFW96,97 simulate with high resolution a handful of individual halos. The fact that we analyze a statistically large sample consisting of dozens of galaxy-size halos in each simulation allows us to make conclusions about *average* halo properties and estimate the amount of cosmic scatter. A summary of the numerical simulations is given in Table 2. The parameters listed in this table are defined in the text above.

### 3.2. Tests of numerical effects

There are several effects which can affect the halo density profiles at scales larger than some particular scale related to this effect. We have tested the reliability of the simulated density and velocity profiles by comparing results of the simulations with different resolutions and time steps. Specifically, the tests were used to determine the range of numerical parameters for which the convergence of density profiles was found at scales larger than two formal resolution elements (formal resolution is equal to the

size of the refinement mesh cell).

Tests presented in Kravtsov et al. (1997) show that the density profiles are not affected by the force resolution down to a scale of about one resolution element (a similar conclusion was reached by NFW96). To test the effects of the time step we have used a set of  $64^3$ -particle simulations of the CDM model with parameters identical to those described in the previous section. These test simulations were started from identical initial conditions, but evolved with different time steps:  $\Delta a_0 = 0.006, 0.003, 0.0015, 0.00075$ . Comparison of the density profiles for the *same* halos in these simulations shows that for halos of all masses, the profiles converge for runs with  $\Delta a_0 \lesssim 0.0015$  (the value used in our CDM and  $\Lambda$ CDM simulations) at all scales, down to the resolution limit. We further use two  $128^3$ -particle simulations of the  $\Lambda$ CDM model with the box size of  $15h^{-1}$  Mpc and with time steps of  $\Delta a_0 = 0.006$  and  $\Delta a_0 = 0.0015$ . The comparison shows that the most massive halos (virial mass  $M_{vir} > 10^{13} h^{-1} M_\odot$ ) have systematically shallower central ( $r \lesssim 10-20h^{-1}$  kpc) density profiles in the  $\Delta a_0 = 0.006$  run as compared to the halos from the  $\Delta a_0 = 0.0015$  run. However, the difference decreases with decreasing halo mass and for  $M_{vir} \lesssim 5 \times 10^{12} h^{-1} M_\odot$  the density profiles from the two runs are identical within statistical noise at scales larger than one resolution element. This mass dependence is due to the different accuracy of numerical integration in objects of different masses. The accuracy depends on the average displacement of particles during a single time step: for the integration to be accurate, the displacement should be  $\lesssim 10 - 20\%$  of the resolution element. Particles inside more massive halos have considerably higher velocities ( $v \gtrsim 300 - 400$  km/s) and thus average displacements that are larger than the displacements of particles inside small halos ( $v \lesssim 200$  km/s). In this study we focus on the mass distribution of the small halos ( $M \lesssim 1 \times 10^{12} M_\odot$ ), for which the tests indicate convergence of the density profiles for time steps  $\Delta a_0 \leq 0.006$ . The time step of all simulations presented in this paper, except for the CHDM simulation, is *four times smaller* than the above value (see Table 2). As an additional test, we have compared average RC shapes for CDM halos in the  $7.5h^{-1}$  Mpc box simulation shown in Figure 2a and for halos in the same mass range ( $\lesssim 1 \times 10^{12} M_\odot$ ) from an identical simulation (identical initial conditions and simulation parameters) with time step  $\Delta a_0 = 0.006$ . We have found that average RC shapes and the scatter in these two simulations are indistinguishable.

The mass resolution in our simulations (particle mass) is  $\sim (0.6 - 5) \times 10^7 h^{-1} M_\odot$  for  $L_{box} = 7.5h^{-1}$  Mpc runs, and  $1.3 \times 10^8 h^{-1} M_\odot$  for the test  $L_{box} = 15h^{-1}$  Mpc  $\Lambda$ CDM run (see Table 2). Therefore, halos of mass  $M_{vir} = 10^{12} h^{-1} M_\odot$  and  $M_{vir} = 10^{11} h^{-1} M_\odot$  (the range of masses used in our comparison with the data) are resolved with  $\sim 100,000$  and  $\sim 10,000$  particles, respectively. For reference, there are  $\gtrsim 100 - 200$  particles inside the innermost point (2 formal resolutions) of the rotation curve used in the fitting procedure described below. Comparison of the average velocity profiles in the  $\Lambda$ CDM<sub>7.5</sub> and  $\Lambda$ CDM<sub>15</sub> simulations (the latter has *eight times* worse mass resolution than the former) shows that there are no systematic differences between profiles in these two runs

TABLE 2  
PARAMETERS OF THE NUMERICAL SIMULATIONS

Model	$\Omega_0$	$\Omega_\Lambda$	$\Omega_\nu$	$h$	$\sigma_8$	$z_i$	$\Delta a_0$ $\times 10^{-3}$	$L_{box}$ $h^{-1}$ Mpc	Particle mass $\times 10^7 h^{-1} M_\odot$
CDM	1.0	0.0	0.0	0.5	0.7	40	1.5	7.5	5.56
$\Lambda$ CDM <sub>7.5</sub>	0.3	0.7	0.0	0.7	1.0	40	1.5	7.5	1.67
$\Lambda$ CDM <sub>15</sub>	0.3	0.7	0.0	0.7	1.0	30	1.5	15.0	13.3
CHDM	1.0	0.0	0.2	0.5	0.7	30	6.0	7.5	4.44 <sup>a</sup> 0.56 <sup>b</sup>

<sup>a</sup>cold particles; <sup>b</sup> hot particles.

(see Fig.2).

The force resolution can introduce errors in rotational velocities. To estimate this effect, we assume that the finite force resolution results in a flat core ( $\rho = \text{const}$ ) at scales smaller than the resolution element  $h_r$  in an otherwise ideal NFW halo (Eq. [1]). This results in the velocity profile  $v_{soft}(r)/v_s = \sqrt{f(x)/xf(1)}$ , where  $f(x) \equiv x_h^2/3(1+x_h)^2 + F(x) - F(x_h)$ ,  $F(x) \equiv \ln(1+x) - x/(1+x)$ ,  $x \equiv r/r_s$ ,  $x_h \equiv h_r/r_s$ ,  $v = v(r_s)$ , and  $r_s$  is the scale-radius of the NFW profile (Eq. [1]). This profile can be compared with the velocity profile corresponding to Eq. (1):  $v_{NFW}(r)/v_s = \sqrt{F(x)/xF(1)}$ . The error is  $\sim 18\%$  at  $r \approx h_r$ , and  $\lesssim 5\%$  at  $r \gtrsim 2h_r$  (see Fig. 5). Thus, the velocity profiles of simulated halos should not be significantly affected at scales  $r \gtrsim 2h_r$ , which is where we perform the fit to analytic models.

To test whether the box size of our simulations ( $7.5h^{-1}$  Mpc) is large enough not to miss all important tidal effects, we have compared the density and velocity profiles of halos formed in  $\Lambda$ CDM<sub>7.5</sub> and  $\Lambda$ CDM<sub>15</sub> simulations. We have not found any systematic differences between halo density profiles in these simulations. The average profiles of halos are identical within the statistical noise (see Figure 2). We have also used another indirect way of testing for the proper simulation of the tidal fields. Tidal torques from the surrounding large-scale structure presumably play a major role in the acquisition of the angular momentum,  $J = |\mathbf{J}|$ , by the galaxy-size halos (Peebles 1969; Doroshkevich 1970). Therefore, we can test if the tidal effects were simulated properly by comparing the so-called spin parameter for the halos in our runs with previous results based on the larger-box simulations. The spin parameter,  $\lambda$ , of a halo is defined as  $\lambda \equiv J|E|^{1/2}/(GM^{5/2})$ , where  $J$  is the angular momentum of the halo,  $E$  is its total energy, and  $M$  is the halo virial mass. We have found that the distributions of  $\lambda$  is very nearly log-normal<sup>4</sup>,  $P(\lambda) = (1/\lambda\sqrt{2\pi}\sigma) \exp(-\ln^2(\lambda/\lambda_*)/2\sigma^2)$ , with  $\lambda_* \approx 0.047, 0.045$ , and  $0.048$  and  $\sigma \approx 0.66, 0.55$ , and  $0.62$ , for the CDM,  $\Lambda$ CDM, and CHDM models respectively. Our results are in good agreement with previous studies (e.g., Barnes & Efstathiou 1987; Warren et al. 1992; Cole & Lacey 1996; Thomas et al. 1997). We therefore conclude that our simulations properly include all essential

tidal effects.

### 3.3. Results

We have used a halo-finding algorithm described in Kravtsov et al. (1997) to identify halos in the simulations at  $z = 0$ . The algorithm identifies halos as local maxima of mass inside a given radius. The exact center of a halo is found iteratively. We have run tests to ensure that we determine the halo center and resulting central density profile correctly. Only halos with more than 1000 particles within their virial radius<sup>5</sup>,  $r_{vir}$ , were taken from the full list. Also, to avoid effects of ongoing mergers we excluded those halos which have close ( $r < r_{200}$ ) companions of mass more than half of the halo mass.

The circular velocity profiles,  $v(r) = [GM(r)/r]^{1/2}$ , were constructed by estimating the mass inside concentric spherical  $\Delta = 1h^{-1}$  kpc shells around the halo center. To avoid contamination by gravitationally unbound background particles, we iteratively remove all particles which have velocities relative to the velocity of the halo as a whole greater than escape velocity. The escape velocity,  $v_e(r)$ , at a given distance  $r$  from the halo center is computed analytically assuming that density distribution follows NFW profile (eq. 1):  $v_e(r) = \sqrt{-2\phi(r)} \approx 2.15 v_{max} \sqrt{\ln(1+2x)/x}$ , where  $\phi(r)$  is halo gravitational potential at the distance  $r$ ,  $v_{max}(r_{max})$  is the maximum rotation velocity of halo and  $x \equiv r/r_{max}$ . This is a good approximation for a large range of  $r$ : NFW96 show that profile (1) approximates the density and velocity profiles of halos reasonably well at scales  $\sim (0.01 - 1)r_{vir}$  (see also Fig.5). The maximum rotation velocity  $v_{max}$  and corresponding scale  $r_{max}$  are found from a halo velocity profile at each iteration. The analysis shows that unbound particles affect at most the outer regions of halos<sup>6</sup>,  $r \sim (0.5 - 1)r_{vir}$ , while inner regions are virtually unaffected (Klypin, Gottlöber, & Kravtsov 1997).

To compare the shape of the observed and simulated dark matter velocity curves, we have fitted the latter with the analytic model described by equation (3). The parameters  $\alpha$ ,  $\beta$ , and  $\gamma$  were fixed at the values used to fit dwarf and LSB galaxies – 2, 3, and 0.2 correspondingly, and we have fitted for the remaining two free parameters –  $r_0$  and  $\rho_0$ . It should be noted that the observed rotation curves of

<sup>4</sup>Note that the most probable value of this distribution is  $\lambda_{\text{peak}} = \lambda_* \exp[-\sigma^2] \sim 0.032$  for the fit values quoted.

<sup>5</sup>According to predictions of the spherical top-hat collapse model we define the virial radius as radius of a sphere encompassing a mean overdensity of 200 for CDM and CHDM models, and 340 for  $\Lambda$ CDM model (Lahav et al. 1991; Kitayama & Suto 1996; Gross et al. 1997).

<sup>6</sup>The case, for example, for a small halo located at the outskirts of a larger system, or for two halos passing close to each other.

most dwarf and LSB galaxies are measured only to radii of  $\lesssim 10 - 30h^{-1}$  kpc and often are still rising at the last measured point. Therefore, the mass distribution in the outer parts of the galactic halos (and often maximum rotation velocity) is poorly constrained. To avoid any bias in the fitting procedure we considered only the inner  $30h^{-1}$  kpc of the simulated halos. We then normalized each rotation profile to its best fit values of  $r_0$  and rotational velocity  $v_0$  at  $r_0$  and computed the average of these normalized profiles over all halos considered in each cosmological model ( $\sim 50 - 60$ ). In Figure 2 we compare the average normalized dark matter velocity profiles for halos formed in CDM,  $\Lambda$ CDM, and CHDM models, shown by solid lines, with corresponding profiles of the dwarf galaxies from our sample, shown with different symbols (the symbols are as in Fig.1). The average profile from the larger-box  $\Lambda$ CDM<sub>15</sub> simulation is shown with a dashed line. This profile does not extend to values of  $r/r_0$  which are as low as for the  $\Lambda$ CDM<sub>7.5</sub> profile (due to worse spatial resolution). However, for values of  $r/r_0$ , where the two profiles overlap, they are indistinguishable. The dotted lines show the  $2\sigma$  envelope representing the scatter of individual halo profiles around the average. It should be noted that the scatter in the inner regions of the halo velocity profiles is substantial. This scatter possibly reflects physical differences between individual halos: our tests show that it is unlikely that the scatter can be attributed to the statistical noise associated with the finite mass resolution. The mass resolution of our simulations is very high (see Table 2): the number of dark matter particles inside the smallest scale,  $r_{min}$ , of rotation curve used in the fitting procedure is  $\gtrsim 200$  for large ( $\sim 10^{12} M_\odot$ ) halos and  $\gtrsim 100$  for smaller ( $\sim 10^{11} M_\odot$ ) halos.

Figure 2 shows that *on average* the velocity profiles of halos formed in hierarchical structure formation models and observed dark matter halos are in good agreement. It also shows that both cold dark matter halos and halos of dark matter dominated galaxies exhibit a certain self-similarity of the mass distribution in their inner regions. It was noted previously (e.g., B95, NFW96) that hierarchical formation of the halos should also result in well-defined scaling properties of the mass distribution. It is thus interesting to compare the scaling properties of galaxy halos in our sample with those of the DM halos formed in the three hierarchical models studied in this paper. Figure 3 shows the plot of the best-fit parameters  $r_0$  and  $\rho_0$  of the model density distribution (3) for the dwarf (solid circles) and LSB (open circles) galaxies together with corresponding parameters of DM halos formed in CDM (a),  $\Lambda$ CDM (b), and CHDM (c) simulations. As before, the values of the remaining parameters of the profile (3) were fixed to  $(\alpha, \beta, \gamma) = (2, 3, 0.2)$ . For both galaxies and simulated halos, the parameters  $r_0$  and  $\rho_0$  are clearly correlated: the halos that are compact are systematically denser. DM halos in all models are fairly consistent with the observational points, except possibly for the CDM model that appears to form halos somewhat denser than observed. Note that the absence of halos at  $r_0 \lesssim 2h^{-1}$  kpc is due to our finite numerical resolution rather than the generic failure of these models to produce very compact halos. The characteristic density of the DM halos correlates strongly with halo mass in a way that reflects the mass dependence of the epoch of

halo formation (NFW96): low-mass small halos collapse at systematically higher redshifts (when the universe was denser) and are therefore denser than the larger higher-mass halos. Thus, the correlation observed in Figure 3 is likely to reflect the different formation epochs of individual halos.

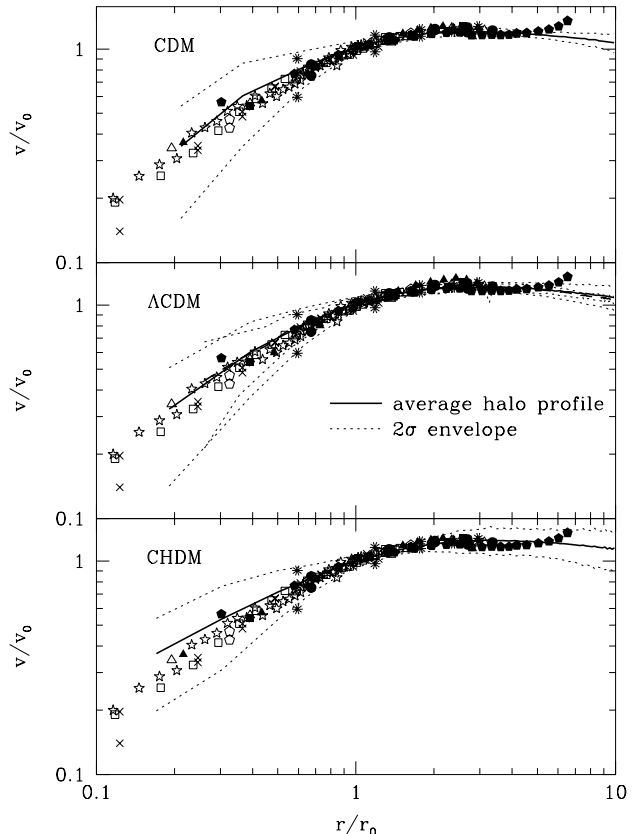


FIG. 2.— Average normalized dark matter velocity profiles for halos formed in (*top panel*) CDM, (*middle panel*)  $\Lambda$ CDM, and (*bottom panel*) CHDM models with corresponding profiles of the dwarf galaxies from our sample. The dotted lines show the  $2\sigma$  envelope representing scatter of individual halo profiles around the average. It should be noted that although the velocity profiles of the hierarchically formed dark matter halos are on average consistent with the shape of observed rotation curves, the scatter in the inner regions of the halo velocity profiles is substantial. This scatter possibly reflects real physical differences between individual halos. The average profile from the larger-box  $\Lambda$ CDM<sub>15</sub> simulation (with 2 times worse spatial and 8 times worse mass resolutions) is shown with a dashed line in the middle panel. This profile does not extend to values of  $r/r_0$  which are as low as for the  $\Lambda$ CDM<sub>7.5</sub> profile (due to worse spatial resolution). However, for values of  $r/r_0$ , where the two profiles overlap, they are indistinguishable. This suggests that the shape is not affected by the finite size of the simulation box and mass resolution. The peculiar upturn in the rotation curve of NGC2915 is discussed in §2.2.

A similar correlation can be observed in the  $r_{max} - v_{max}$  plane, shown in Figure 4 (values of  $r_{max}$  and  $v_{max}$  for each galaxy are given in Table 1). The maximum point in a galaxy's DM velocity profile and the corresponding radius is a nice set of physical parameters for comparison with simulations. Ideally, such a comparison would not force any pre-supposed fit to either the data or the simulated profiles. Unfortunately, most of the galaxy rotation



curves in our sample do not extend to  $r$  large enough to explicitly define the maximum velocity. Therefore, we find  $v_{max}$  by fitting the velocity profile  $V(r)$  in eq. (4) using parameters which produce a velocity curve equivalent to the  $\rho(r)$  fits discussed above:  $(a,b,g) = (1.5, 0.34, 0.9)$ . After each galaxy is fit with this profile, we use the fit to determine its maxima. We have, in a sense, tested this procedure with a mock run with the simulated halos: we performed the same fit to the inner profiles of the simulated halos ( $r < 30h^{-1}\text{kpc}$ ) and then compared this to the maxima determined using a smooth (all parameters free) fit *over all radii* of the halos. The values of  $v_{max}$  found by these two methods are virtually identical. Although there is some scatter between the corresponding values of  $r_{max}$ , there is no systematic difference between the two. The rms difference in values of  $r_{max}$  (determined by the two fitting procedures) is smaller than the scatter from halo to halo at any particular  $v_{max}$ .

We see from Figure 4 the trend that larger  $r_{max}$  correspond to larger  $v_{max}$ . Such a trend was also seen in NFW96 (their Fig.10). Note that when the  $h$  factor is scaled out of the  $r_{max}$  axis, the three models lie very closely along each other in this plot. But since the observationally determined radii of the galaxies depend on  $h$ , the plots show the differences accordingly.

Note that we have fitted  $\gamma = 0.2$  from the observed galaxies rather than a value derived from the simulations because of the larger scatter in the latter. However, if we fix  $\alpha = 2$  and  $\beta = 3$  we can attempt to find the best-fitting ranges of  $\gamma$  for each of our simulated models. The procedure for finding best-fit gamma values for the halos is not entirely straightforward since, depending on the the mass of the halo (and intrinsic scatter), the characteristic scale  $r_0$ , may be as small as the resolution limit, and the inner-slope will be poorly constrained. That is, if we were to fix  $\alpha = 2$  and  $\beta = 3$  and fit the value of  $\gamma$  freely for each halo, the smaller halos ( $M \lesssim 10^{11}M_\odot$ ) would not offer any strong constraint, and the fitting routine could yield spurious or unphysical values for  $\gamma$ . What we have done instead is compared the “stacking” of halos for a range of  $\gamma$  values (0-1.5). We fit each halo using logarithmic radial binning out to the virial radius, and only fit radii which were greater than twice the formal resolution. This bin spacing emphasizes the inner profile shape. After fitting each halo for a particular value of  $\gamma$  (with  $(\alpha, \beta) = (2,3)$ ) we normalized each by  $r_0$  and  $\rho_0$  and effectively plotted them on top of each other. The scatter in this stack is a nice way of determining how well the imposed profile shape fits a set of halos. This procedure also allows us to treat large halos (which, within resolution, probe  $r/r_0 \ll 1$ ) and small halos equivalently. Using this criteria, we find that the ranges  $\gamma_{\Lambda\text{CDM}} \approx 0 - 0.4$ ,  $\gamma_{\text{CDM}} \approx 0 - 0.5$ , and  $\gamma_{\text{CHDM}} \approx 0 - 0.7$  provide the best fits.

#### 4. DISCUSSION

The most important conclusion evident from the results presented in the previous section is that there is *no statistically significant discrepancy between the shapes of rotation curves of simulated halos and rotation curve shapes of galaxies in our sample*. This conclusion is somewhat surprising in light of the previous results (Flores & Primack 94; Moore 1994; NFW96) that indicated a significant discrepancy between numerical simulations and ro-

tation curve measurements. We see at least two possible explanations for the controversy. First, both Moore (1994) and NFW neglected the fact that distances to these galaxies (and thus the physical scales of the rotation curves) are very poorly determined (with a typical error of  $\sim 50\%$  or more; L. van Zee, private communication). With a distance uncertainty this large, it is hardly legitimate to make a raw comparison of the profiles at a specific physical distance scale. The comparison between rotation curves of dwarf galaxies and different analytic models was made by B95. The comparison was made, however, in units of  $r/r_b$  (see eq.(2)), in which case the uncertainty in distance in both  $r$  and  $r_b$  cancels out in the ratio (the same is true for our analysis that was done in units of  $r/r_0$ ). Indeed, the discrepancy between the analytic model (1) and the data (Fig.1 in B95) was not as large as was found by Moore (1994). Note that the study by Flores & Primack (1994) was also done using dimensionless scale units:  $r/b_{HI}$ , where  $r$  is the physical scale of the rotation curves and  $b_{HI}$  is the *HI* disk scale length. The key point is that the rotation curve *shape* is independent of the uncertain distance to the galaxy.

The second possible source of discrepancy concerns the procedure followed to compare the numerical results with observations. When comparing to the RC data, we have used  $(\alpha, \beta, \gamma) = (2, 3, 0.2)$  fit (motivated by the observed galaxies’ RCs; see Fig.1) only to determine  $r_0$  and  $v_0$  for the inner halo RCs (i.e.,  $r \leq 30h^{-1}\text{kpc}$ ) so that these can be properly rescaled and compared to the dwarf RCs in Fig. 2. Other authors compare the data to a simple analytic fit to the entire halo profile (i.e.,  $r \lesssim r_{vir}$ ), e.g.  $\rho_{\text{NFW}}(r)$ . Therefore, when compared to the data, any deviations of actual halo profiles from analytic fit were neglected. Although the universality of the mass distribution in the DM halos is most likely real and reflects the self-similar nature of their formation, the associated scatter of the real profiles should not be neglected. Also, possible systematic deviations (especially in the inner,  $r \lesssim r_0$ , regions) of the actual profiles from the analytic model (1) should be kept in mind. Our analysis shows that such deviations do, in fact, exist. Figure 5a shows the velocity profiles of a sample of the DM halos in our CDM simulation normalized to their best fit values of the characteristic radius  $r_s$  and rotational velocity at  $r_s$ . Figure 5b shows residuals between the halo velocity profiles and the analytic fit by the NFW profile. All profiles are shown down to their spatial resolution. Figure 5b shows that the halo rotational velocities at scales  $r/r_s \lesssim 0.5$  are systematically lower than the rotational velocities predicted by the best fit NFW profile. Fig. 5 shows that  $\rho_{\text{NFW}}(r)$  is a rather good fit to our halos for  $r \gtrsim 0.03r_{vir}$ , but not for the smaller scales that are relevant to observed inner rotation curves. Figure 6 in NFW96 and Figure 4 in NFW97 show that similar deviations seem to exist in their simulations as well. It was suggested (J. Navarro, private communication) that the inner density distribution may depend on the dynamical state of the halo: the most relaxed halos may have systematically steeper inner density profiles. We do not find such a trend for the halos analyzed in this paper. There does not seem to exist any correlation of the inner slope of the density profiles or the concentration parameter,  $c \equiv r_{vir}/r_s$ , with the dynamical state of the halo

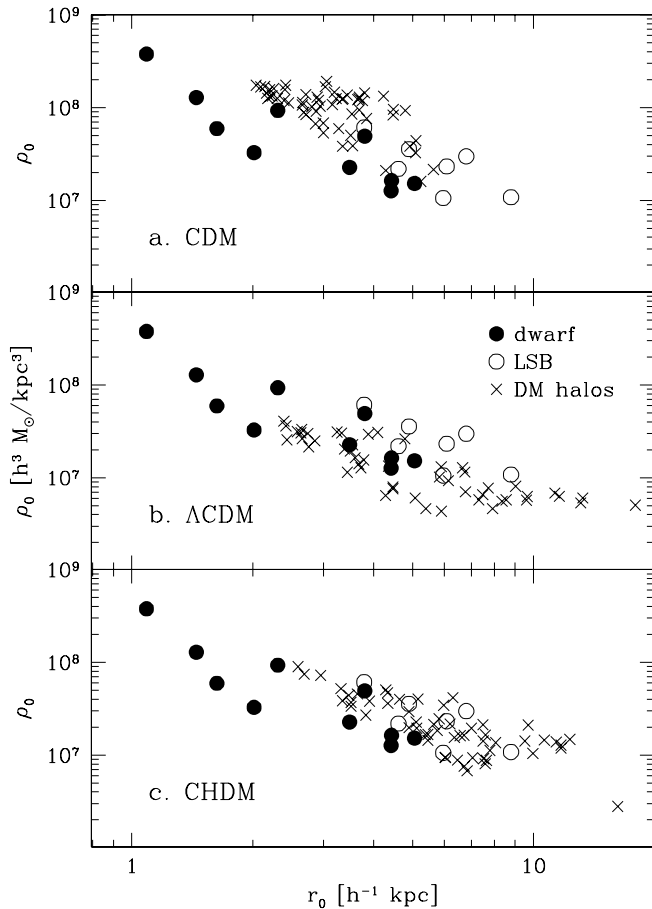


FIG. 3.— Correlation of the best-fit parameters  $r_0$  and  $\rho_0$  for the dwarf and LSB galaxies (solid and open circles, respectively) and for the dark matter halos (crosses) formed in (a) CDM, (b)  $\Lambda$ CDM, and (c) CHDM models. The correlation is consistent with the correlations of simulated DM halos: smaller halos are denser.

quantified by the fractional difference between the center of mass inside the halo virial radius and the halo center (the density peak):  $d_{CM} = |\mathbf{r}_{peak} - \mathbf{r}_{CM}|/r_{vir}$ . However, if a weak correlation does exist, it could be lost due to the rather large errors in determining  $c$  ( $\sim 30\%$ ) for small halos ( $M_{vir} \sim 10^{11} - 10^{12} h^{-1} M_\odot$ ). Our analysis shows that although the whole ensemble of the halo profiles can be described reasonably well by a fixed set of the parameters  $\alpha$ ,  $\beta$ , and  $\gamma$ , the scatter in these parameters among the individual halos is substantial. Thus, for example, the average velocity profiles of halos shown in Figure 2 are very close to the observational points, whereas the upper  $2\sigma$ -envelopes (the dotted lines) lie considerably higher in the inner regions of the rotation curves. The discrepancy between the analytic model of NFW and the data found by B95 is actually within  $\lesssim 1\sigma$  from our average halo profiles. The scatter is not caused by poisson noise: the halo rotation curves contain  $\gtrsim 100$  particles inside the innermost bin used in the fitting. There are different possible sources of this scatter. The set of parameters  $(\alpha, \beta, \gamma) = (2, 3, 0.2)$ , used to make a sensible comparison between data and models in the  $r/r_0 - v/v_0$  plane may not be the best description of the mass distribution in the simulated halos. However,

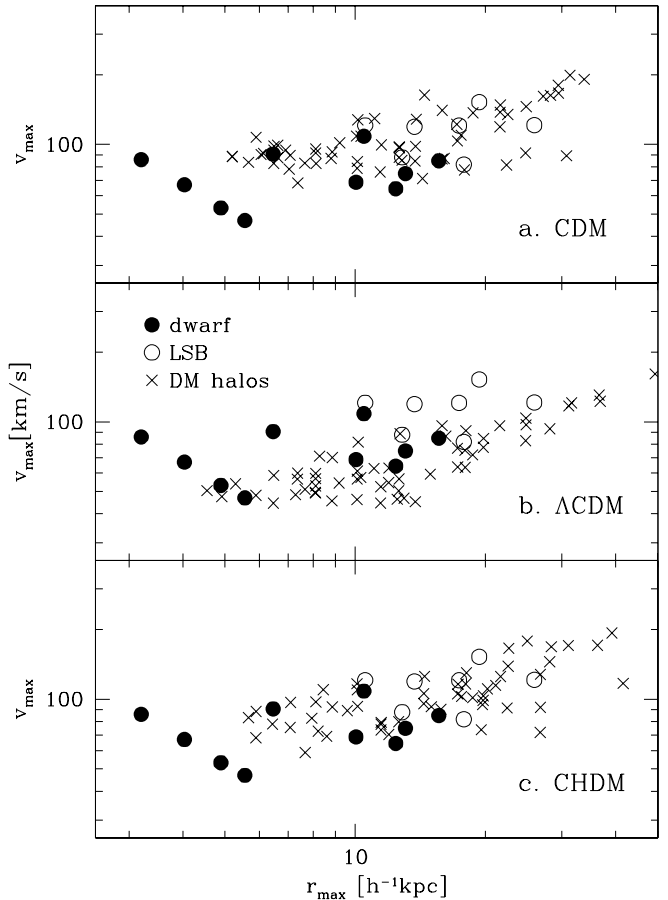


FIG. 4.— Correlation of the maximum velocity of the rotation curves,  $v_{max}$ , and scale at which this maximum occurs,  $r_{max}$ , for observed galaxies and simulated DM halos (the symbols are the same as in Fig.3).

our analysis shows that the true source is probably real differences between mass distributions of different halos. For example, when we allow parameter  $\alpha$  vary freely with other parameters fixed to  $\gamma = 0.2$  and  $\beta = 3$ , this results in a wide range of best fit values for  $\alpha$  ( $\sim 0.7 - 2$ ). Also, the density distribution in the inner regions varies substantially from halo to halo: the density profiles of some halos are considerably steeper than profiles of the others. We can thus talk only about “approximate universality” of the profiles and some amount of scatter will be introduced with any fixed set of parameters. Regardless of the nature of this scatter, it should not be neglected when making comparisons with the data. And it is this scatter which makes us conclude thus it is premature to claim a discrepancy between the mass distribution of hierarchically formed halos and observed rotation curves of dark matter dominated galaxies.

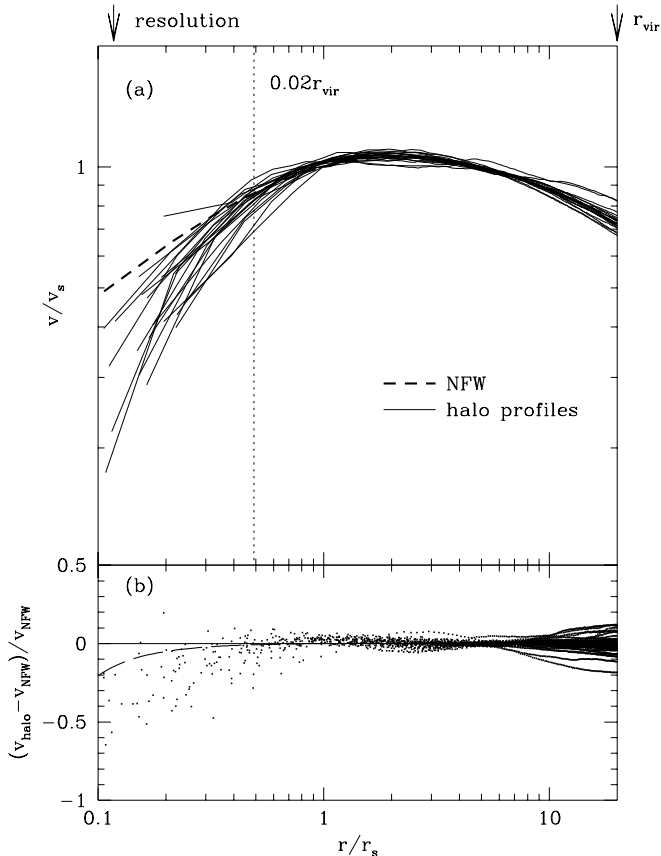


FIG. 5.— (a) Velocity profiles of the DM halos in our CDM simulation normalized to their best fit values of the NFW profile: the characteristic radius  $r_s$  (see eq.[1]) and the rotational velocity at  $r_s$  (the actual values of these parameters for the halos used are in the range  $r_s \sim 4 - 10h^{-1}$  kpc and  $v_s \sim 120 - 200h^{-1}$  km/s depending on the halo’s virial mass). The dashed line shows the RC predicted by the NFW analytic density profile (eq. [1]). (b) Residuals between the halo velocity profiles and the analytic fit by the NFW profile. All profiles are shown down to their spatial resolution. Note that although the NFW profile provides a reasonably good fit at  $0.5 \lesssim r/r_s < 20$  (corresponding approximately to  $0.02 \lesssim r/r_{vir} < 1$ ), the rotational velocities of halos at scales  $r/r_s \lesssim 0.5$  are systematically lower than the rotational velocities predicted by the NFW profile. The long-dashed curve shows errors in rotation velocity due to the force softening, assuming the NFW profile (see §3.2). The errors due to softening are  $\lesssim 5\%$  at the scales that were used in fitting ( $x \gtrsim 0.2$ , corresponding approximately to two resolution elements) and cannot account for  $\sim 5 - 10$  times larger deviations from the NFW profile observed at these scales.

Although it appears that we cannot reject any of the analyzed cosmological models, we note that the cores of DM dominated galaxies are potentially very useful probes of both the history of galaxy formation and the underlying cosmological model. The inner regions of DM halos are expected to be very sensitive to the merging history. The accretion of small dense satellites builds up a cuspy inner density profile after only few mergers (Syer & White 1997), even if the initial density profile had a flat core. The slope  $\gamma$  is expected to be a function of the merger rate and the slope of the perturbation spectrum on scales corresponding to the mass of a halo. This result can be

used possibly to constrain models. According to the analysis of Syer & White (1997), the steeper the slope of the power spectrum  $n$  ( $P(k) \propto k^n$ ), the shallower the central density profile:  $\gamma \approx 3(3+n)/(5+n)$ . If this result is qualitatively correct, the shallower slope of  $P(k)$  at cluster scales ( $n \sim -2$ ), as compared to the slope at galactic scales ( $n \sim -2.5$ ), should result in steeper central density profiles for cluster-size halos. The rotation curves of galaxies in our sample suggest a slope of  $\gamma \sim 0.2 - 0.4$ . These values, according to the analysis of Syer & White, correspond to spectrum slopes of  $n \approx -2.9$  and  $n \approx -2.7$ . Note that  $n_{\text{CDM}} \approx -2.4$ ,  $n_{\text{ACDM}} \approx n_{\text{CHDM}} \approx -2.6$  on the scales of the halos that we analyze. The slope  $\gamma$  may potentially be a useful probe of the spectrum. Note that our simulations show a considerable spread in the slopes of the central density profiles. The physical processes which lead to differences in the central density profiles seen in our halos (e.g., environment, dynamical state, etc.) are not clear and will be investigated in a future study.

Navarro, Eke, & Frenk (1996) suggested that the cores of dwarf galaxies may also be sensitive to possible past violent star formation bursts in these galaxies. They showed that a sudden loss of most of a galaxy’s gas, blown away in the course of a star formation burst, may lead to formation of a flat core, even if the initial density distribution was coreless. However, the parameters used to model such an event were somewhat extreme, and it is not clear whether this mechanism would work for most of the dwarf galaxies. Moreover, a significant fine tuning would be required to explain the observed degree of self-similarity of the mass distribution in the dwarf galaxies. In this paper we showed that mass distribution in the LSB galaxies is, in fact, very similar to the mass distribution of the dwarf galaxies. This makes it even harder to explain such regularity with this mechanism alone, because many of the LSB galaxies are fairly massive systems which are unlikely to have lost much of their gas in starbursts.

Recently, Burkert & Silk (1997) used an improved rotation curve measurement of the dwarf DDO154 to argue that discrepancy between the NFW profile and the observed mass distribution in this galaxy can be explained by a dark spheroid of baryons with mass several times the mass of the observed disk and comparable to the mass of the cold dark matter halo. This hypothesis must be tested using other galaxies and observations of the MACHOs in our galaxy that constitute the main observational evidence for the existence of such massive baryonic halos. The observed self-similarity of the mass distribution in the dark matter dominated galaxies which we analyze requires that the distribution of the baryonic dark matter be self-similar too and suggests a certain degree of “conspiracy” between baryonic DM and cold DM halos. The results presented in this paper show that the mass distribution in our hierarchically formed cold dark matter halos is consistent with the dynamics of the dark matter dominated galaxies and we think that it is somewhat premature to invoke an additional dark matter component. However, if further results on the distribution of MACHOs shows that the mass contribution of these objects is substantial, the possibility of such a component must be taken into account. Note also that, as we discussed in §2.2, the rotation curves of two of the dwarf galaxies, DDO154 and NGC2915, show a peculiar behavior at large radii that cannot be described

by any smooth model of density distribution.

## 5. CONCLUSIONS

To summarize, our results are the following.

- Rotation curves of DM dominated dwarf and LSB galaxies have a similar shape. This shape is inconsistent with  $\rho_{NFW}(r)$  (eq. [1]), but is well fit by the coreless profile described by eq. (3) which has a shallower slope at small scales:  $\rho(r) \propto 1/r^\gamma$ ,  $\gamma \approx 0.2 - 0.4$ , corresponding to a steeply rising velocity curve [ $v(r) \propto r^g$ ,  $g \approx 0.9 - 0.8$ ].
- We find that *on average* the velocity profiles of the halos formed in the hierarchical structure formation models analyzed in this paper (CDM,  $\Lambda$ CDM, and CHDM) and observed dark matter halos are in reasonably good agreement. We find a substantial amount of scatter in the central density profiles of individual halos around the average. The physical processes which lead to differences in the central density profiles seen in our halos (e.g., environment, dynamical state, etc.) are not clear and will be the subject of a future study.

- The inner ( $r < 30h^{-1}$  kpc) average density profiles of DM halos in all of our simulations are well fit by model (3) with  $(\alpha, \beta, \gamma) = (2, 3, 0.2)$ , and equivalently the rotation curves are well described by RC (4) with  $(a, b, g) = (1.5, 0.34, 0.9)$ . The profiles systematically deviate from the NFW profile (1) at small scales.
- We find that dark matter dominated dwarf and LSB galaxies show correlations between their characteristic density and radius consistent with the correlations of hierarchically formed DM halos: physically smaller halos are denser. We find a similar correlation between the maximum of the rotation curve,  $v_{max}$ , and the corresponding radius  $r_{max}$ .

We would like to thank Erwin de Blok and Liese van Zee for sending us rotation curves in the electronic form. This work was supported by NASA and NSF grants at NMSU and UCSC. JSB acknowledges support from a GAANN predoctoral fellowship at UCSC and thanks the Northern California Association of Phi Beta Kappa for a graduate scholarship. Simulations reported here were done at NMSU, NCSA (at the University of Illinois), and Hebrew University.

## REFERENCES

- Barnes, J., & Efstathiou, G. 1987, ApJ, 319, 575  
 Bottema, R. 1997, A&A, 328, 517  
 Burkert A. 1995, ApJ, 447, L25  
 Burkert, A., & Silk, J. 1997, ApJ, 488, 55  
 Casertano, S., & van Gorkom, J.H. 1991, ApJ, 101, 1231  
 Carignan, C., & Freeman, K. C. 1988, ApJ, 332, L33  
 Carignan, C., & Beaulieu, S. 1989, ApJ, 347, 760  
 Carignan, C., Côté, S., Freeman, K.C., & Quinn, P.J. 1997, AJ, 113, 1585  
 Cole, S., & Lacey, C. 1996, MNRAS, 281, 716  
 Côté, S., Carignan, C., & Sancisi, R. 1991, AJ, 102, 904  
 Courteau, S., & Rix, H.-W. 1997, A&AS, 191, 7702  
 de Blok, W.J.G., & McGaugh, S.S. 1997, MNRAS, 290, 533  
 de Blok, W.J.G., McGaugh, S. S., & van der Hulst, J.M. 1996, MNRAS, 283, 18  
 Doroshkevich, A.G. 1970, Astrofizika, 6, 581  
 Dubinski, J., & Carlberg, R. 1991, ApJ, 378, 496  
 Flores, R., & Primack, J.R. 1994, ApJ, 427, L1  
 Gross, M.A.C., et al., 1997, in preparation  
 Jobin, M., & Carignan, C. 1990, AJ, 100, 648  
 Hockney, R.W., & Eastwood, J.W. 1981, Computer simulations using particles (New York: McGraw-Hill)  
 Kitayama, T., & Suto, Y. 1996, ApJ, 469, 480  
 Klypin, A.A., Gottlöber, S., & Kravtsov, A.V. 1997, ApJ, submitted  
 Kravtsov, A.V., Klypin, A.A., & Khokhlov, A.M. 1997, ApJS, 111, 73  
 Lahav, O., Lilje, P.B., Primack, J.R., & Rees, M.J. 1991, MNRAS, 251, 128L  
 Lake, G., Schommer, R.A., & van Gorkom, J.H. 1990, AJ, 99, 547  
 Martimbeau, N., Carignan, C., & Roy, J.-R. 1994, AJ, 107, 543  
 Meurer, G.R., Carignan, C., Beaulieu, S.F., & Freeman, K.C. 1996, AJ, 111, 1551  
 Moore, B. 1994, Nature, 370, 629  
 Navarro, J.F., Frenk, C.S., & White, S.D.M. 1996, ApJ, 462, 563  
 Navarro, J.F., Frenk, C.S., & White, S.D.M. 1997, ApJ, 490, 493  
 Peebles, P.J.E. 1969, ApJ, 155, 393  
 Persic, M., Salucci, P., & Stel, F. 1996, MNRAS, 281, 27  
 Primack, J.R., Holtzman, J., Klypin, A., Caldwell, D.O. 1995, Nuclear Phys., B43, 133.  
 Syer, D., & White, S.D.M. 1998, MNRAS, 293, 337  
 Thomas, P.A. et al. 1997, MNRAS, submitted (astro-ph/9707018)  
 Tully, R.B. 1988, Nearby Galaxies Catalog (Cambridge: Cambridge Univ. Press)  
 van Zee, L., Haynes, M.P., Salzer, J.J., & Broeils, A.H. 1997, AJ, 113, 1618  
 Warren, M.S., Quinn, P.J., Salmon, J.K., & Zurek, W.H. 1992, ApJ, 399, 405  
 Zaritsky, D., Smith, R., Frenk, C.S., & White, S.D.M. 1997, ApJ, 478, L53  
 Zaritsky, D., & White, S.D.M. 1994, ApJ, 435, 599  
 Zhao, H.S. 1996, MNRAS, 278, 488